A novel 3φ solar power-driven PV inverter system for stand-alone applications PV Grid Connected Converter

[1]Konda Naresh,[2]Ch Sreenu,
[1]Assistant Professor, [2]Assistant Professor,
[1]Electrical; Engineering of Department,
[2]Electrical; Engineering of Department, Hyderabad, India.

Abstract : In study, a novel 3φ solar power-driven PV inverter system for stand-alone applications. Considering that high PV side voltage causes several drawbacks, a low voltage PV source is utilized as a part of the proposed system. The constraint of low-voltage PV source is overcome by utilizing a unique high voltage- increase front-end dc–dc converter fit for working at high effectiveness and MPPT. The proposed plan is especially helpful for long battery life by as it guarantees no battery over charge or discharge, For this reason, the customary MPPT plan is replaced by RPT, which guarantees that just the required voltage is followed from the PV source. This averts the drawing of overabundance voltage from the PV source and the utilization is more then we prefer "dump" loads. Not just the primary power organize additionally the battery interfacing bidirectional stage likewise underpins high voltage pick up with high productivity. A dual inductor step-up Push-Pull active clamped is investigated in this paper, presenting PSIM 9.0/MATLAB simulation and equipment results for passive and active over voltage clamping the prototype of the investigated converter is elaborated for 1200W power to match the rated power of the PV/Fuel cell active clamped technology have been investigated in research laboratory.

***Keywords*-PV cell; DC-DC Converter; Current-fed; Soft Switching.**

I. INTRODUCTION

Details the background and literature for converter control schemes, power transfer theory, control of ac current and ac voltage using PWM techniques. The synchronization process and control of dc link voltage is explained. Fig.4.1 shows system integration of PV inverter system which comprises of a PV panel, associated with a dc-dc converter and a widely used dc-ac pulse width modulation (PWM) inverter connected to the utility grid. Amirabadi *et al.* [24] have proposed a stand-alone PV system based on a multiport high-frequency ac link inverter. The high-frequency ac link reduces the harmonics in the ac output current of the inverter. A drawback of the system is the use of relatively high PV and battery voltage. Another stand-alone PV system with battery backup, based on a novel three-port dc–dc converter has been proposed by Chen *et al.* [25] for dc loads. The advantage of this system is that low-voltage PV and battery can be used, integrated through the same high-gain converter. However, the control flexibility is low because of the complexity of the converter. Caracas *et al.* [26] have proposed a battery less standalone solar PV system for water pumping application using a high-voltage-gain dc–dc converter stage in the system.

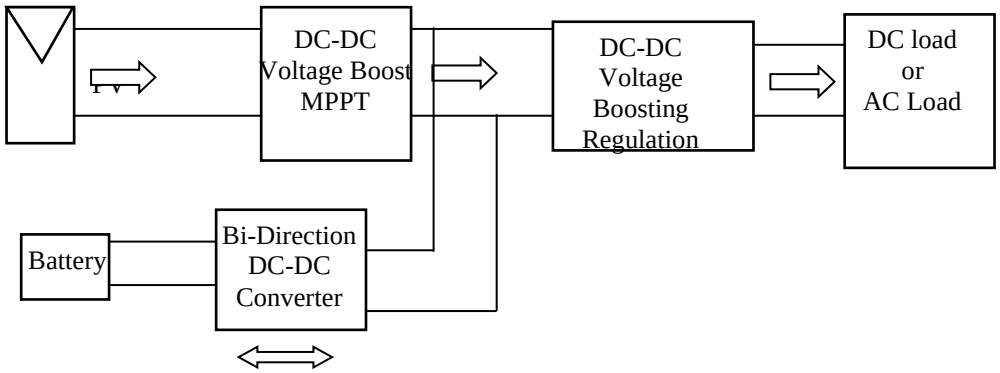

Fig.1.1 Block diagram of a Two-Stage Stand-alone PV System

In accordance with the ongoing discussion, this paper presents a novel configuration that overcomes the stand-alone PV systems' drawbacks described in the preceding paragraphs.

The proposed two-stage PV power conversion system for standalone ac loads has the following features.

1) It has a novel front-end dc–dc power conversion stage with high voltage gain capability. In spite of the required high voltage gain (40–400 V, i.e., a gain of ≈ 10), the efficiency (≈ 96%) is not compromised. A conventional dc–dc converter would give much lower efficiency for this kind of gain.

2) The front-end dc–dc stage is capable of performing both electrical MPPT and the required power tracking (RPT) of the PV source depending on the load requirement and the battery state of charge (SOC). RPT capability obviates the dump load requirement.

3) A BESS is interfaced through another high-gain high efficiency bidirectional converter. In conjunction with RPT, the battery charge is strictly regulated to ensure its life.

4) The control strategy proposed in this paper ensures fast transient response, low harmonics, and small steady-state errors with a simple and compact control.

5) This system can be easily upgraded to higher power rating by interfacing additional renewable energy sources with the dc link.

II. PV SYSTEM ANALYSIS

The efficiency of the converter is around 96%, which increases the overall efficiency of the stand-alone system. The RPT of the PV source is implemented by varying the duty cycle of the switch (*S*) of the converter as per the RPT algorithm described in the next section. RPT also contributes to the increased efficiency of the system. The circuit schematic of the bidirectional converter used in the battery interface is shown in Fig. 4.2(b). On the other hand, during the charging of the battery, i.e., flow of power from the dc link toward the battery, it works as a buck converter. The duty cycles of the converter during the buck and boost modes are denoted by d_{buck} and d_{boost}, respectively.

The control scheme of the bidirectional dc–dc converter maintains the SOC level of the battery between SOC_{min} < SOC <SOC_{max} based on the reference load power and the PV generated power. The expression for voltage gain of this converter, when the battery supplies power to the dc link, is given by

$$\frac{V_{dc}}{V_{bat}} = \frac{n+1}{1-d_{boost}}$$

Where V_{bat} denotes the battery voltage. During charging of the battery, the voltage gain of the converter is given by

$$\frac{V_{bat}}{V_{dc}} = d_{buck}$$

The efficiency in the boost mode is observed to be around 96%, where as in the buck mode, it is around 94%.

1) Low losses in the switch (low conduction loss, low switching loss due to zero voltage switching

2) energy recovery from leakage inductance, and

3) operating the converter at nominal duty cycle.

same leg.

$$\frac{T}{T_s} = \frac{V_{carrier} - V_{moculation}}{V_{carrier}}.$$

The average voltage at any time is:

$$V_{average} = \frac{T_s - T}{T_s} \times \frac{V_{dc}}{2} = \frac{V_{modulation}}{V_{carrier}} \times \frac{V_{dc}}{2} = M \times \frac{V_{dc}}{2} \quad (1.1)$$

Where the modulation index, M, varies with time to synthesize the average voltage. If the average voltage were plotted, it would look like the modulating voltage waveform (inverter sine output). The output voltage of the VSI does not have the shape of the desired signal, but switching harmonics, can be filtered out by the series LCL low pass filter, to retrieve the 50Hz fundamental sine wave.

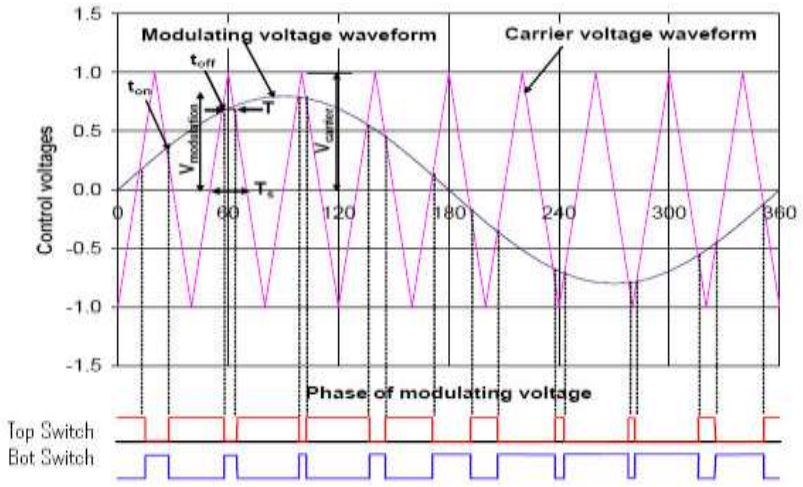

Figure: 2.1: Key Waveforms One phase of control voltage waveforms to modulate pulse widths

A .Photovoltaic Cell and Array Modeling

PV cell is a simple p-n junction diode which converts solar irradiation into electricity. Fig. 2.13 shows an equivalent circuit diagram of a PV cell which consists of a light-generated current source I_L, a parallel diode, a shunt resistance R_{sh}, and a series resistance R_s.

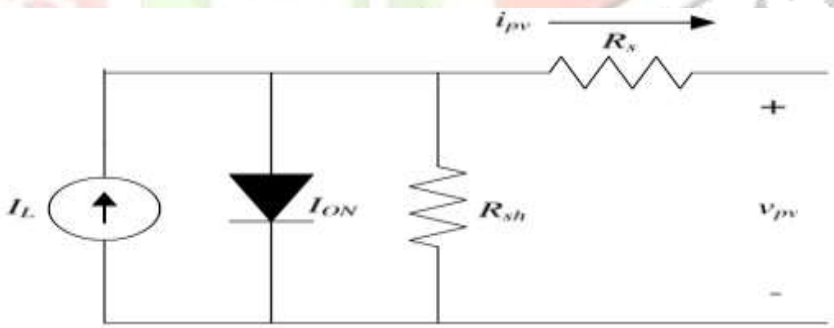

Figure: 2.2 Equivalent circuit diagram of PV cell

$$I_{ON} = I_s = \left[exp\left[\alpha\left(v_{pv} + R_s i_{pv}\right) - 1\right]\right] \quad (2.1)$$

Where $\alpha = q/AkTC$, k = 1.3807 × 10−23 $J.K^{-1}$ is the Boltzmann's constant, q = 1.6022 × 10−19 C is the charge of electron, *A* is the p-n junction ideality factor whose value is between 1 and 5, I_s is the saturation current, and v_{pv} is the output voltage of PV array, which in this case is the voltage across *C*, i.e., v_{dc}.

Now, by applying Kirchhoff's current law (KCL) in Fig. 2.12, the output current i_{pv} generated by PV cell can be written as

$$i_{pv} = I_L - \left[exp\left[\alpha\left(v_{pv} + R_s i_{pv}\right) - 1\right]\right] - \frac{v_{pv}+R_s i_{pv}}{R_{sh}} \quad (2.2)$$

The light-generated current I_L depends on the solar irradiation which can be related by the following equation:

$$I_L = \left[I_{sc} + k_i\left(T_c - T_{ref}\right)\right]\frac{s}{1000} \quad (2.3)$$

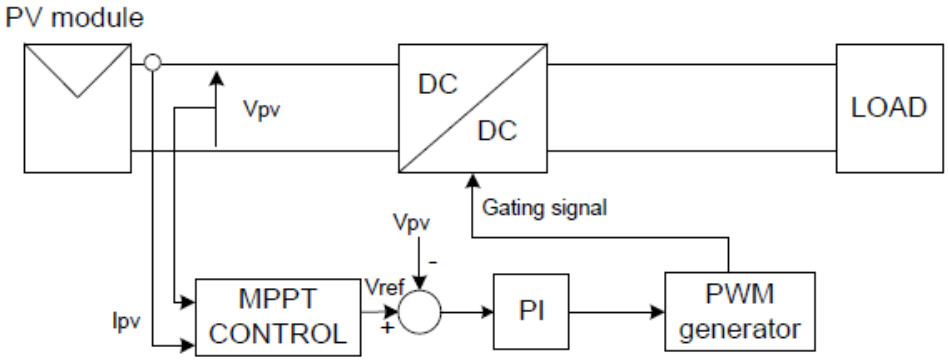

Figure:2.3: Block diagram of MPPT with P&O

For Hill moving, there is no controller, just the obligation proportion controls the converter specifically as appeared in Fig.

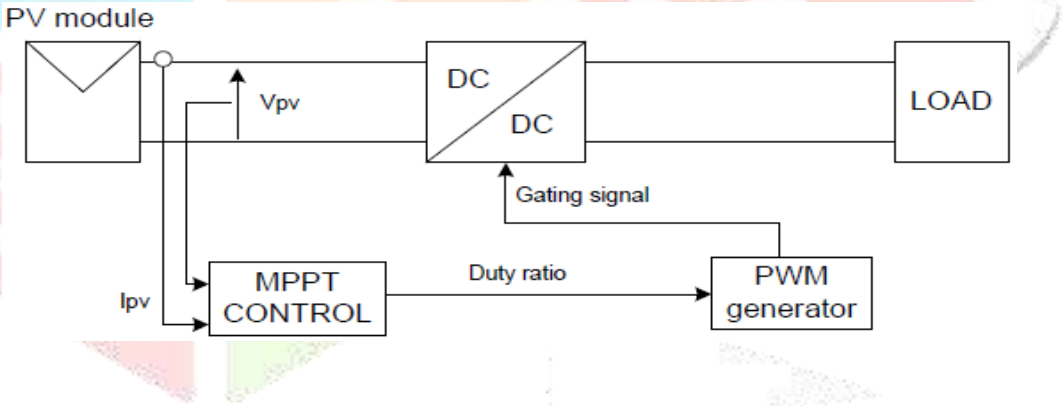

Figure:2.4: Block diagram of MPPT with Hill Climbing

In Fig. 3.5, it can be watched that augmenting the PV voltage expands the force of the PV and decrementing the PV voltage diminishes the force of the PV when working on the left of the MPP. On the privilege of MPP, augmenting the voltage diminishes the force and decrementing the voltage expands the force. This procedure will be actualized in the MPPT controller to remove

The following set of equations describes the incremental conductance algorithm:

$$P = V \times I \quad (2.3)$$

Deriving Equation (3.3) with respect to *V*:

$$\frac{dP}{dV} = \frac{d(V\times I)}{dV}$$

$$\frac{dP}{dV} = I\frac{dV}{dV} + V\frac{dI}{dV}$$

$$\frac{dP}{dV} = I + V\frac{dI}{dV} \tag{2.4}$$

Since it is known that:

$$\frac{dP}{dV} = 0 \tag{2.5}$$

At the MPP, combining Eqn (3.4) and Eqn (3.5) and substituting $\frac{I}{V} = G$, with G being the conductance, the following relationship is established:

$$\frac{dI}{dV} = -\frac{I}{V}$$

$$\frac{dI}{dV} = -G \tag{2.6}$$

If the incremental changes dV and dI are approximated by comparing the most recent measured and approximated to

$$dV(k) \approx V(k) - V(k-1)$$

$$dV(k) \approx \Delta V$$

And $$dI(k) \approx I(k) - I(k-1)$$

$$dI(k) \approx \Delta I$$

Finally the algorithm can be summed up in the following set of equations.

$$\frac{dP}{dV} > 0, \rightarrow G > \Delta G \tag{2.7}$$

$$\frac{dP}{dV} = 0, \rightarrow G = \Delta G \tag{2.8}$$

$$\frac{dP}{dV} < 0, \rightarrow G < \Delta G \tag{2.9}$$

The incremental conductance can determine that the MPPT has reached the MPP and stop perturbing the operating point. If this condition is not met, the direction in which the MPPT operating point must be perturbed can be calculated using the relationships describes in Eqn (3.7) and Eqn (3.9).

$$\left|\frac{dI}{dV} + \frac{I}{V}\right| \leq \varepsilon \tag{2.10}$$

It consists of a coupled inductor($L_1 \parallel L_2$), a passive clamp network (C_1,D_1), and an intermediate energy storage capacitor (C_2), which helps to increase voltage gain without the need for an exorbitantly high duty cycle. The high voltage at the dc link (V_{dc} in Fig. 4.2) is achieved by the voltage step-up property of the coupled inductor ($L_1 \parallel L_2$). The leakage energy of the coupled inductor is recovered by the passive clamp network (C_1,D_1). The voltages of the coupled inductor and the clamp capacitor are added to charge the intermediate energy storage capacitor (C_2), which results in a significant increase of the output voltage (i.e., high voltage gain).The voltage gain expression for this converter is derived by applying volt-second balance across $L1$ as follows:

$$V_{L1(ON)}d + V_{L1(OFF)}(1-d) = 0.$$

The expression for the voltage gain of this converter is given by

$$m = \frac{V_{dc}}{V_{PV}} = \frac{n+1}{1-d}$$

V. SIMULATION

A $3-\emptyset$ ac ($155\mathbf{V_{ph}}$) load was considered for simulations. Corresponding to this, a PV source of about 1000 W at 1000 W/$\mathbf{m^2}$ (MPP) was simulated. The PV source is able to maintain a voltage between 40 and 60 V as the radiation varies from 500 to 1000 W/$\mathbf{m^2}$. Up to 500 W/$\mathbf{m^2}$, the dc link reference voltage $\mathbf{V^*}$ dc can be maintained at 400 V. As the radiation falls below 500 W/ $\mathbf{m^2}$, the $\mathbf{V^*}$ dc value must be reduced, as explained in the previous section. The following sequence of events was simulated, and the corresponding waveforms are shown in Fig.6.4. At time, *t* = 0 s, it is assumed that the PV source is receiving 1000W/m2 and the battery is 100% charged. Full 675-W load is present. Since $\mathbf{P_{PV} > P_{desired}}$ and the battery is fully charged, the control scheme performs RPT, drawing only 700Wfrom the PV source (against an available PV power of 1000W). This is substantiated by the simulation waveforms in Fig. 9(a).

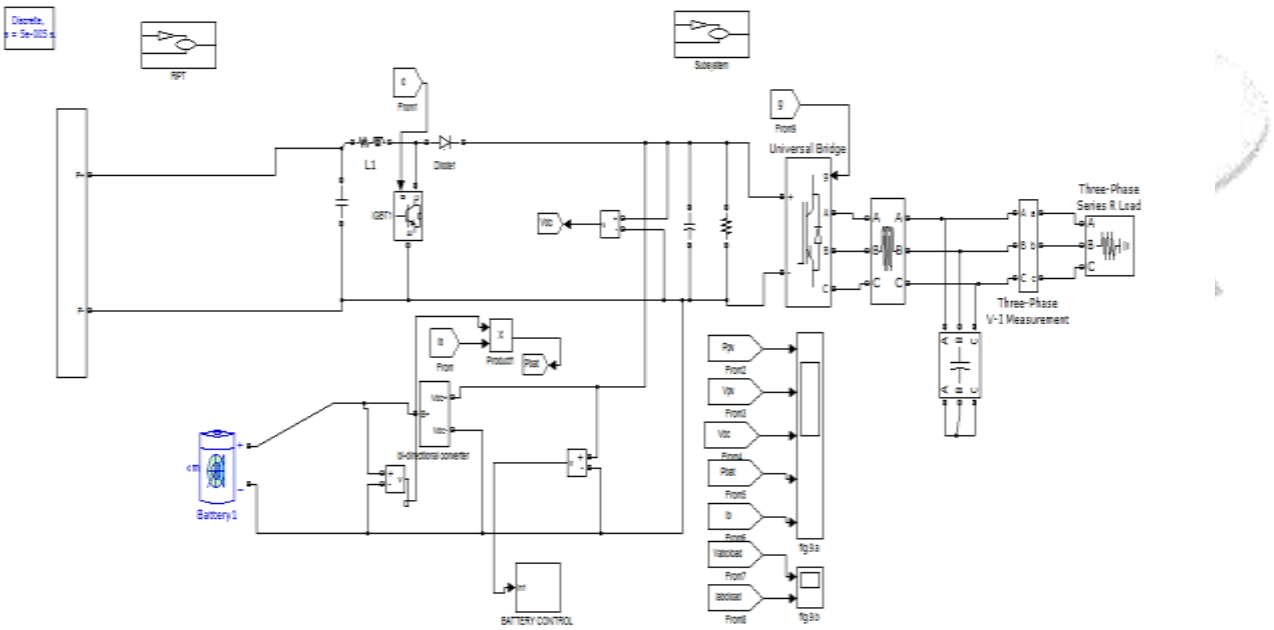

Figure: 5.1 .Block diagram showing the complete system and the control signals.

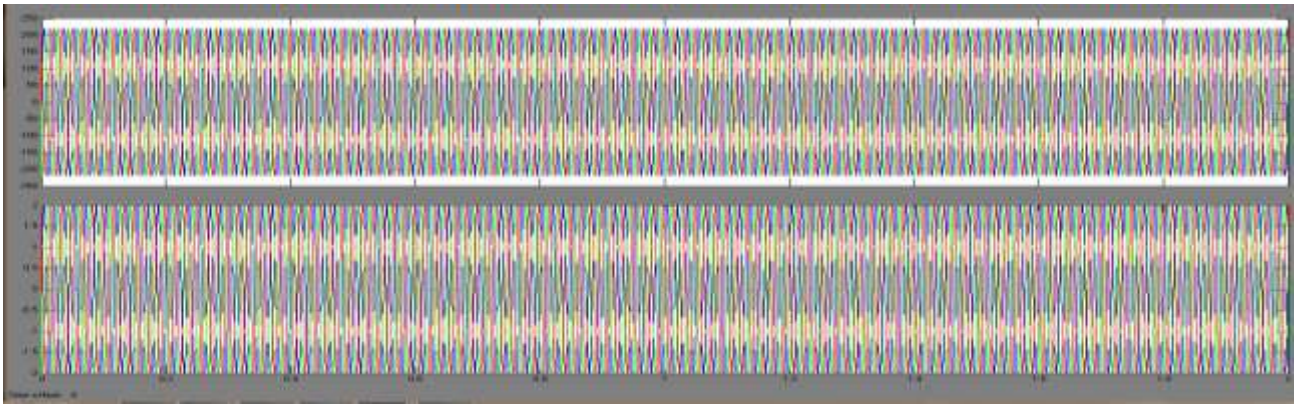

Figure: 5.2. (b)Simulation results of the proposed system across load

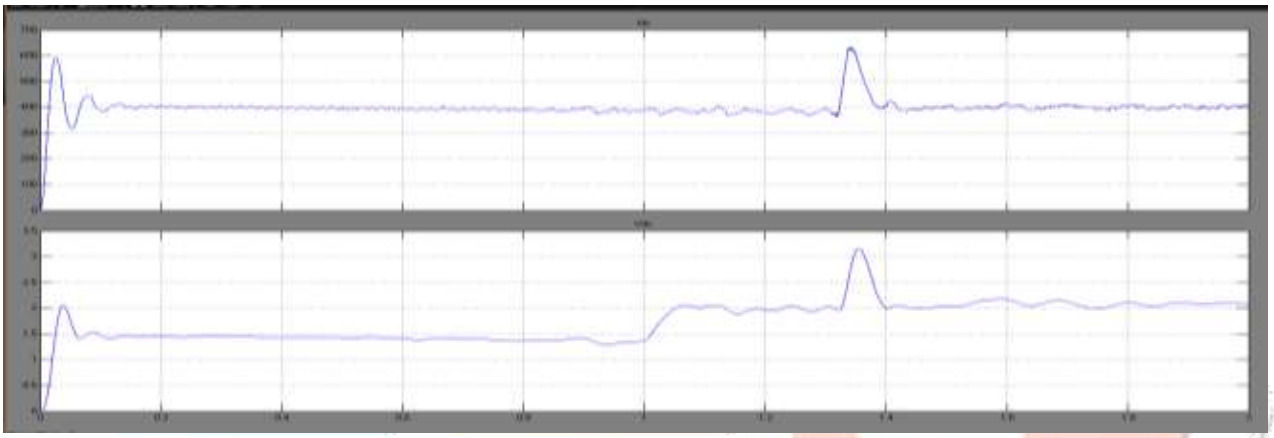

Figure:5.3 (a).Dynamic Response to step change in effective load

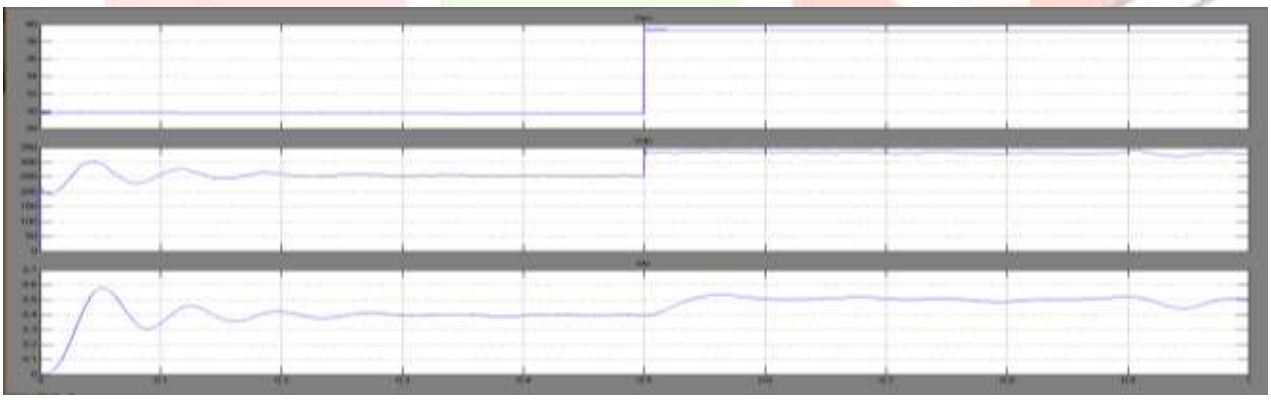

Figure: 5.3(b).Dynamic Response to step change in reference dc link voltage

The proposed control scheme was simulated in MATLAB/Simulink software. It was subsequently validated on a laboratory also. But while comparing fig.6.4 and fig.6.7. The fuzzy based results have high performance when compare to traditional controllers. Here we use PI controller as traditional controller. The fuzzy and PI difference is normally shown in the curve plotted for V_{dc}.The distortions were very less when we simulated with fuzzy controller.

V.CONCLUSION

This paper has proposed and actualized a novel 3φ solar powered PV inverter system for stand-alone applications. Considering that high PV side voltage causes several drawbacks, a low voltage PV source is utilized as a part of the proposed system. The constraint of low-voltage PV source is overcome by utilizing a unique high voltage- increase front-end dc–dc converter fit for

working at high effectiveness and MPPT. The proposed plan is especially helpful for long battery life by as it guarantees no battery over charge or discharge, For this reason, the customary MPPT plan is replaced by RPT, which guarantees that just the required voltage is followed from the PV source. This averts the drawing of overabundance voltage from the PV source and the utilization is more then we prefer "dump" loads. Not just the primary power organize additionally the battery interfacing bidirectional stage likewise underpins high voltage pick up with high productivity.

The control goals had been dissected and it is inferred that the control loop must give exact phase and amplitude regulation. In this way a present control loop with PI controller is proposed.

The extension of this work might focus on the following aspects:

- Feedback control of the dc-link voltage ripple.

REFERENCES

[1] S. Lee, G. Son, and J.-W. Park, "Power management and control for grid-connected DGs with intentional islanding operation of inverter," IEEE Trans. Power Systems, vol. 28, no. 2, pp. 1235–1244, May 2013.

[2] P. Xuewei and A. K. Rathore, "Small Signal Modeling of Snubberless Soft-switching Current-fed Bidirectional Converter and Control Implementation using PSoC," IEEE Transactions on Vehicular Technology, vol. 64, no. 11,Nov 2015, pp. 4996-5005.

[3] Ravi Bukya and Prof B.Mangu, "Soft-Switching Snubberless Current fed half bridge DC-DC Converter For PV Application" IEEE Conference on ICITE-2018 ,Apr-18.

[4] Shih-Jen Cheng; Yu-Kang Lo; Huang-Jen Chiu; Shu-Wei Kuo, "High- Efficiency Digital-Controlled Interleaved Power Converter for High- Power PEM Fuel-Cell Applications," IEEE Transactions on Industrial Electronics, vol.60, no.2, pp.773-780, Feb. 2013.

[5] P. Xuewei and A. K. Rathore, "Naturally Clamped Zero Current Commutated Soft-switching Current-fed Push-Pull DC/DC Converter: Analysis, Design, and Experimental Results," IEEE Transactions on Power Electronic, Vol. 30, no. 3, March 2015, pp. 1318-1327.

[6] S. Bal, A. K. Rathore, and D. Srinivasan, "Naturally commutated current-fed three-phase bidirectional soft-switching dc-dc converter with 120^o modulation technique," *in Press, IEEE Transactions on Industry Applications, Jan 2016.*

[7] S. Bal, A. K. Rathore, D. Srinivasan, "Naturally clamped snubberless soft-switching bidirectional current-fed three-phase push-pull dc/dc converter for dc microgrid application," *IEEE Transactions on Industry Applications*, vol. 52, no. 2, March/April 2016, pp. 1577-1587.